EUROPEAN ORGANIZATION FOR NUCLEAR RESEARCH

Proposal to the ISOLDE and Neutron Time-of-Flight Committee

Collinear resonance ionization spectroscopy of silver between $N = 50$ and $N = 82$

May 13, 2020

R. P. de Groote,[1] M. L. Bissell,[2] T. E. Cocolios,[3] B. S. Cooper,[4] K. T. Flanagan,[2,4] S. Franchoo,[5] R. F. Garcia Ruiz,[6] R. Heinke,[3] J. Johnson,[3] Á. Koszorús,[7] Y. C. Liu,[8] G. Neyens,[3,9] F. P. Gustafsson,[3], C. M. Ricketts,[2] M. Reponen,[1] S. W. Bai,[8] A R. Vernon,[3] S. G. Wilkins,[10] X. F. Yang[8]

[1]*Department of Physics, University of Jyväskylä, PB 35(YFL) FIN-40351 Jyväskylä, Finland*

[2]*School of Physics and Astronomy, The University of Manchester, Manchester M13 9PL, United Kingdom*

[3]*KU Leuven, Instituut voor Kern- en Stralingsfysica, B-3001 Leuven, Belgium*

[4]*Photon Science Institute Alan Turing Building, University of Manchester, Manchester M13 9PY, United Kingdom*

[5]*Institut de Physique Nucléaire Orsay, IN2P3/CNRS, 91405 Orsay Cedex, France*

[6]*Massachusetts Institute of Technology, Cambridge, MA 02139, USA*

[7]*Department of Physics, University of Liverpool, Liverpool L69 7ZE, United Kingdom*

[8]*School of Physics and State Key Laboratory of Nuclear Physics and Technology, Peking University, Beijing 100871, China*

[9]*Physics Department, CERN, CH-1211 Geneva 23, Switzerland*

[10]*Engineering Department, CERN, CH-1211 Geneva 23, Switzerland*

Spokesperson: R. P. de Groote [rdegroot@cern.ch]
Contact person: M. L. Bissell [mark.lloyd.bissell@cern.ch]

CERN-INTC-2020-023 / INTC-P-551
13/05/2020

Abstract: We propose to measure the electromagnetic moments, nuclear spins and charge radii of exotic silver ($Z = 47$) isotopes using the Collinear Resonance Ionization Spectroscopy (CRIS) method. Using this technique, we can cross the neutron shell closure at $N = 50$ and can closely approach the shell closure at $N = 82$. From the proposed measurements we shall extract detailed information on the strength of the neutron shell closures, and on the shapes and sizes of isotopes between the spherical Sn ($Z = 50$) isotopes and the strongly deformed isotopes near $Z = 45$.

Requested shifts: 35 shifts, (split into 2 runs over 1 year)

1 Introduction

The region near $Z = 50$ has attracted significant interest in recent years. Featuring long isotopic chains which span two neutron shell closures ($N = 50, 82$), many studies on the strength of these shell closures have been performed using different experimental techniques (see e.g. [1, 2, 3, 4]). The region has also become accessible for *ab-initio* nuclear theory as well [5]. At ISOLDE, laser spectroscopy measurements near $Z = 50$ have focused on tin ($Z = 50$) [3], indium ($Z = 49$) [6] and cadmium ($Z = 48$) [7]. At the Ion Guide Separator On-Line in the Accelerator Laboratory in Jyväskylä, experiments on neutron-rich silver ($Z = 47$) up to $N = 74$ and palladium ($Z = 46$) up to $N = 72$ were also recently undertaken. From such high-resolution optical spectroscopy measurements, magnetic dipole moments, electric quadrupole moments, changes in mean-squared charge radii and nuclear spins are measured in a nuclear model-independent way. Since below the proton shell closure $Z = 50$ the arrangement of the proton orbitals changes, as does the proton-neutron interaction, experimental data for isotopes with $Z < 50$ are crucial to predict (the evolution of) the neutron shell gaps.
In general, the dipole moments provide sensitive information on the purity of the nuclear configurations, and serve as stringent tests for theoretical calculations. Thus, for example the strength of the shell closures at $N = 50, 82$ can be evaluated. The quadrupole moments and changes in mean-squared charge radii will be used to investigate the deformation in the mid-shell region between $N = 50, 82$. A comprehensive picture of the evolution of deformation between the magic tin ($Z = 50$) isotopes and the strongly collective region around and below $Z = 45$ can thus be tracked. Furthermore, neutron-rich silver isotopes feature rich isomerism, and firm spin assignments and isomer identification in this region of the chart are needed to anchor earlier decay spectroscopy studies.

2 Physics Motivation

In addition to these general nuclear structure motivations, there are also several unique features in the silver isotopic chains which we propose to investigate. The odd-A isotopes of silver feature two long-lived states: an $I = 1/2^-$ state, which is the ground state close to stability, but which becomes isomeric going towards $N = 50$ and after $N = 74$, and a high-spin state, with $I = 7/2^+$ or $I = 9/2^+$. Fig. 1 summarizes the magnetic dipole moments of the odd-A silver isotopes. For comparison, selected data for the indium isotopes from the recent CRIS campaigns are also shown.
From the g-factors ($g = \mu/I$), it is clear that in all cases the valence proton sits in the $g_{9/2}$ orbit; however, from $N = 56$ onwards the odd protons couple to form a seniority-3 configuration: $(g_{9/2}^{-3})_{7/2^+}$. A similar conclusion can be drawn based on the magnetic moments of the $I = 5^+$ and $I = 6^+$ states in the even-A silver isotopes. It is not clear how far this unusual proton configuration persists on the neutron-rich side; we thus propose to pin down these spins. The magnetic moments of the $I = 1/2^-$ states are even more puzzling. The magnitude of the magnetic moments confirms the leading configuration of these states contains a proton in the $p_{1/2}$ orbit. Unlike the magnetic moments of the high-spin states, which are quasi-constant except when closely approaching the shell

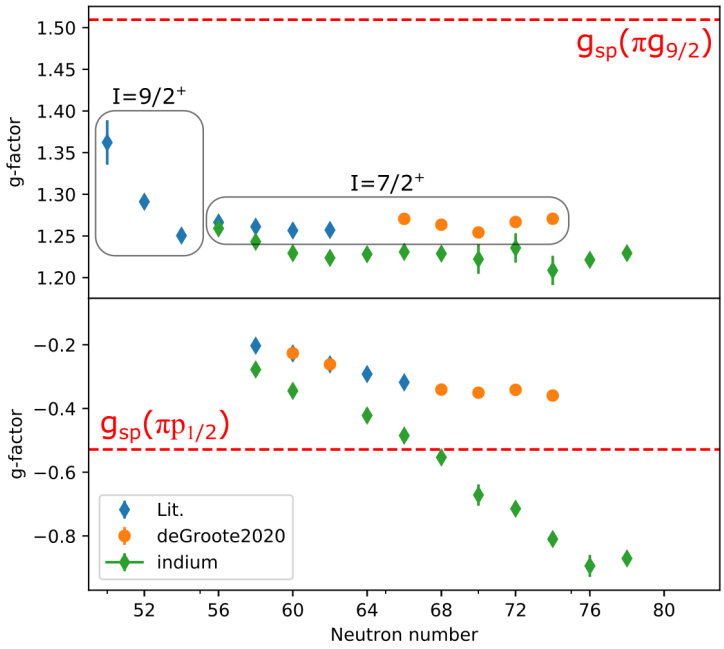

Figure 1: Experimental g-factors of $I = 7/2, 9/2$ and $I = 1/2^-$ states in the odd-A silver isotopes (top and bottom respectively). The red dashed line indicates the effective single-particle g-factor. Literature values for silver are obtained from [8, 9, 10, 11, 12, 13, 14, 1], while results marked as 'deGroote2020' are preliminary IGISOL results. Selected indium g-factors are CRIS results from IS639, soon to be published.

closures, the magnetic moments of the $I = 1/2^-$ states strongly change with neutron number. The slope of this change in the mid-shell appears smaller for the silver isotopes than for the indium isotopes. These observations are currently not understood, since the magnetic moment of $p_{1/2}$-states are insensitive to configuration mixing in the first order. It is of particular interest to the present proposal whether the change in trend and sudden increase at $N = 82$ observed for the indium isotopes [15] is also present in silver, and how the moments change when approaching the other shell closure at $N = 50$. While crossing $N = 50$ for indium is currently out of reach for collinear laser spectroscopy, for silver this is expected to be feasible.

The quadrupole moments provide insight into the development of deformation when moving away from the closed neutron shells. In Fig. 2, the known intrinsic quadrupole moments of the silver isotopes, extracted from the measured spectroscopic moments, are plotted. Uncertainties are dominated by the atomic parameters and reference B-constants, which may be improved with more accurate calculations and a re-measurement of the structure of ^{108m}Ag. By plotting these intrinsic moments rather than the experimentally measured spectroscopic moments, a very consistent picture of the deformation of these isotopes is obtained. We propose to extend these measurements towards the two neutron shell closures $N = 50, 82$, in order to evaluate their respective strengths. Note that the even-A isotopes add important additional information, since several states with $I > 1/2$ can be studied for a given isotope. Comparison with the quadrupole moments and B(E2) values of neighbouring chains will furthermore enable tracking the evolution of collectivity

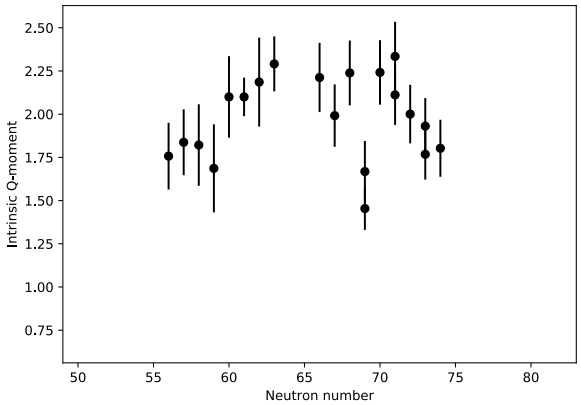

Figure 2: Intrinsic quadrupole moments of the silver isotopes, showing a cohesive picture of the deformation, which appears to be maximal around $N = 65 - 70$.

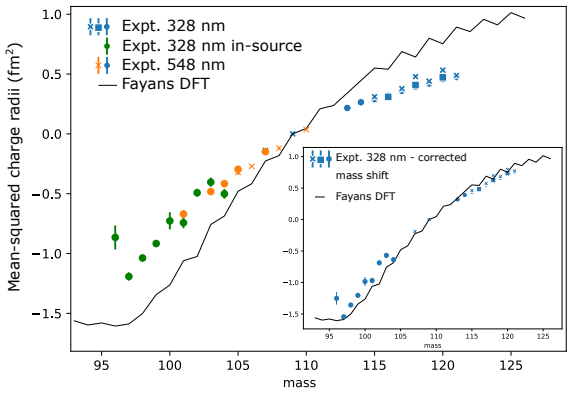

Figure 3: All known mean-squared charge radii of the silver isotopes. EVen close to stability radii of isomeric states are often missing. The inset shows part of the data with an empirically adjusted mass-shift parameter.

when going away from the closed proton shell at $Z = 50$.
Recently, there has been considerable progress in the theoretical description of nuclear charge radii [16, 17, 18, 7, 3]. A global approach, applicable also to heavier systems and systems further removed from closed shells, was found with Density Functional Theory and the development of the Fayans functional. Using nuclear charge radii in the optimization process was demonstrated to be vital to simultaneously reproduce nuanced features such as the odd-even staggering of simultaneously radii and binding energies [17, 19]. Currently, progress is being made on the development of a Fayans functional which offers a description of deformed systems. The silver isotopic chain represents a valuable opportunity to test this new functional, and other theoretical developments in general.
Figure 3 shows the known charge radii of silver isotopes alongside a preliminary calculation using this new Fayans functional. Note that this functional describes neighbouring isotopic chains very well; the mismatch for silver is rather due to inaccurate atomic parameters. Another proposal is submitted to the INTC, which aims to perform muonic X-ray measurements on the long-lived ^{108m}Ag, thus extending the set of absolute charge radii to three isotopes [20]. This third isotope is required for the calibration of the atomic parameters. Alternatively, the atomic parameters could also be adjusted to match the trend of the silver isotopes to Pd and Cd, as was done to produce the inset of Fig. 3. This biased approach may however hide important physics that would otherwise be evidenced by using a nuclear-model independent approach. Note furthermore that for many of the data points in Fig. 3, only one of the long-lived states is shown, irrespective of whether it is the ground or isomeric state, since no data exists for the other(s).
The radioactive neutron-deficient silver isotopes around the $N = Z$ region have also been of considerable interest for several years. These isotopes are of interest due to their proximity to the $N = Z$ line; enhanced proton-neutron correlations may play an important role; the astrophysical rapid-proton (rp-) process passes through this region;

strong shell-correction effects may be expected due to the doubly-magic $N, Z = 50$ shell closure. The spins and moments of both long-lived states in ^{96}Ag, thought to be (2^+) and (8^+), will be very sensitive tests for the purity of the underlying configuration (presumably $\nu g_{9/2} \otimes \pi g_{9/2}$). Similarly, the magnetic moment of the $I = (9/2)$ state in ^{95}Ag will provide an important measure for the purity of the nuclear configuration. Finally, the $N = Z$ isotope ^{94}Ag itself is of interest for a variety of reasons, and has been identified as a key case for future measurement campaigns e.g. using the S3 at GANIL or the MARA-LEB in Jyväskylä.
In addition to general interest in charge radii of self-conjugate nuclei (see e.g. [21, 22]), ^{94}Ag features a unique high-spin $I = (21^+)$ isomer, thought to undergo two-proton decay. Measuring the quadrupole moment and charge radius of this state would provide valuable insight into its charge distribution, and thus provide input for theoretical models. Furthermore, ^{95}Ag also potentially features two long-lived high-spin isomers, tentatively assigned $(23/2^+, t_{1/2} < 16\,\text{ms})$ and $(37/2^+, t_{1/2} < 40\,\text{ms})$ [23]. These isomers likely result from the additional $\pi g_{9/2}^{-1}$ proton hole coupling with the 16^- isomer configuration of cadmium, a theorised proton-emitting spin-gap isomer [24] appearing from lowering in energy of its $\pi g_{9/2}^{-2}$ $\nu g_{9/2}^{-2}$ configuration due to proton-neutron interactions [25]. Measurements on all of these neutron-deficient cases represent an important future step for CRIS at ISOLDE; however, first experiments between $N = 50$ and $N = 82$ are proposed.

3 Experimental details

3.1 Production of silver at ISOLDE

Isotopes near stability and neutron-rich isotopes are best produced by impinging the 1.4 GeV proton beam onto a UC_x target. Figure 4 summarizes the experimental yields reported in [26], and plots them alongside in-target yields calculated using ABRABLA. By scaling these calculated yields down and by furthermore using the release curve information from [26], they can be adjusted to match the experimental data. This can be used to interpolate the approximate yields between ^{121}Ag and ^{129}Ag. Despite the relatively short lifetime of the most neutron-rich isotopes, yields are expected to be above 100 pps between $^{98-127}$Ag. For more neutron-deficient isotopes, a LaC_x target is preferred.

3.2 The CRIS experiment

The measurements of the hyperfine structure of the silver isotopes will be performed using the CRIS method. After mass-separation using the HRS, beams will be injected into the cooler-buncher where they will be cooled, and then ejected as short bunches. These ions will be transported to the CRIS beamline, where they will be neutralized using a hot K vapour. After deflecting the non-neutralized ions, the atoms will be overlapped with several pulsed laser beams. One of these beams will be sufficiently narrowband to resolve the individual hyperfine components. The sequence of laser pulses will ionize the atoms, after which they will be guided onto an ion detector. By counting the number of ions as a function of the frequency of the narrowband scanning laser, the hyperfine structures will be constructed.

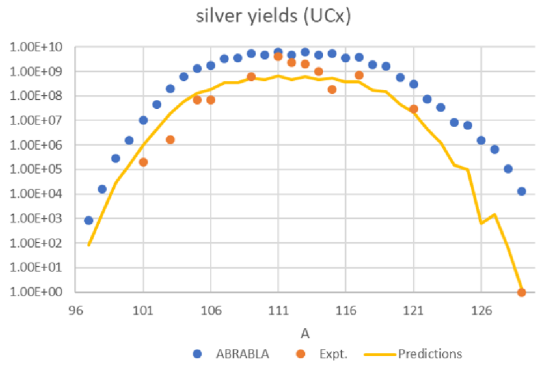

Figure 4: Calculated in-target (blue) and experimental (orange) yields for silver isotopes. The yellow curve shows a yield prediction, taking into account the lifetime of the isotopes.

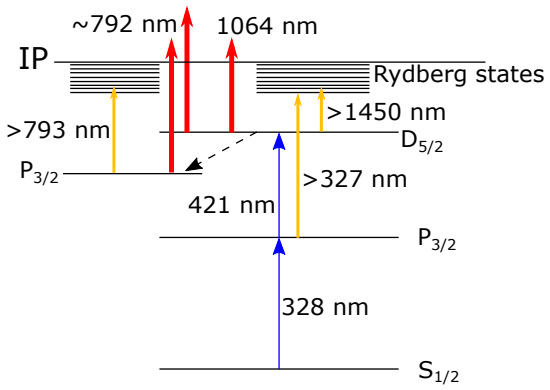

Figure 5: Atomic levels and laser ionization schemes.

3.3 Laser ionization schemes

Two methods of ionizing these atoms will be compared offline, to evaluate their efficiency and the ability to suppress unwanted ionization of contaminants present in the ion beam. The first of these, which uses a high-power laser to excite atoms to just above their ionization potential, has been the standard method for CRIS over the past years. This method provides high ionization efficiencies, but may also non-resonantly laser-ionize contaminants in the beam. The second method, which has been developed offline during LS2 with indium ions, relies on ionizing highly excited silver atoms using strong electric fields instead. This process, called field ionization, is much more selective and furthermore defines a very small ionization volume, which in turn enables a significant suppression of non-resonant collisional ionization of contamination. Silver is an ideal case for this method, as many Rydberg series have been identified, and they have already been demonstrated to be suitable for field ionization.

Possible laser ionization schemes are shown in Fig. 5. The ionization scheme used in recent IGISOL experiments used a three-step 324 + 421 + 792 nm scheme, and was found to be sufficiently efficient to study the very exotic ^{96}Ag using broadband in-source laser spectroscopy. The final step in this scheme was non-resonant. Optical pumping into a high-lying $P_{3/2}$ state could also be observed, and a Rydberg series from this state was also found. Ionization from this state is also possible using the same 792 nm laser, thus boosting efficiency. At CRIS, it is likely a higher efficiency can be obtained using a 1064 nm laser instead, which can provide much higher laser power densities.

There are several options for field ionization. Using the same first and second laser steps, high-power laser beams at wavelengths above $\sim 1.45\,\mu$m, produced using an optical parametric oscillator could be used to excite into high-lying Rydberg states. Alternatively, the use of > 795 nm light to excite the optically pumped atoms into Rydberg states will be tested. Finally, a third option is to use a high-power pulsed dye laser in a two-step scheme, to excite directly from the first excited state into a Rydberg level.

It should be noted that laser resonance ionization has the distinct advantage that a broadband laser can first be used locate resonances in a coarse scan, before zooming in with a narrowband laser system. Since 328 nm is conveniently produced using pulsed dye lasers, this option will be used to speed up resonance searches. This dual-resolution peak searching strategy was used to great effect to find first signals in the RaF molecule [27]. For that experiment, the location of the resonances was only theoretically known with a precision of 30 THz, which meant a huge scan range had to be covered.

4 Yield and shift estimates

In the present proposal, we request shifts to study $^{98-129}$Ag. A future addendum is envisaged to study the neutron-deficient isotopes using a LaC_x target. Ideally, prior to this follow-up, an investigation of the production yields would be performed. In combination with the experience gained from the measurements proposed here, a realistic beam time request could later be drawn up. The requested shifts are summarized in Table 1. In total, 35 shifts are requested.

For all isotopes with a yield above 10^4 per second, data taking times will not be limited by the yield and statistics, but by the time it takes to scan the laser frequency over the required scan range in a repeatable and stable fashion, and the time required for regular reference measurements and corresponding mass-separator mass changes. We therefore count half a shift (4 hours) per isotope. This may seem a conservative estimate, but it should be kept in mind that there are isomeric states present in all isotopes, and that the large hyperfine splitting of silver means large scan ranges need to be covered in order to ensure no states are missed. Note furthermore that we propose to measure the hyperfine structures for all isotopes, including those where literature values are available. This is because in nearly all cases, not all observables were extracted. Furthermore, the current literature values were obtained with different methods, with different experimental setups, and using different optical transitions. A remeasurement of all isotopes is thus required, to ensure no systematic issues are present, in particular for the charge radii.

For isotopes with yields below 10^4 per second, shift requirements were estimated based on previous experiences. For instance, for ^{78}Cu, produced at a rate of 20 pps, one shift was sufficient to scan a frequency range of 2 GHz [28, 19]. For ^{129}Ag, the $I = 1/2^-$ state would likely span a similar frequency range. The $I = 9/2$ $P_{3/2}$ structure would span about 2.5 GHz, organized in two groups which are separated by 40-50 GHz associated with the $S_{1/2}$. Thus, while collecting statistics after the resonances are found would take 4 shifts (1 for $I = 1/2^-$, 2x1.5 for $I = 9/2$), an additional 3 shifts are counted for finding the resonances in a broadband mode.

As a point of comparison for this shift request, for the meaurements performed on neutron-rich and deficient isotopes of indium, in total 12 days were used to measure the properties of 30 isotopes. Similarly to silver, indium features rather large hyperfine spectra and rich isomerism. The shift request presented here for silver is thus justified on the same basis.

Summary of requested shifts: 35 shifts are requested using a UC_x target, split into two runs.

Table 1: Calculated in-target, experimental and predicted yields per μC using a UC_x target. Also listed is the number of states with a lifetime > 1 ms. No shifts are requested for $A < 98$ since those isotopes are likely easier to study using a La_x target.

A	Nr. of states	ABRABLA calc	Expt.	Predicted yield	Shifts
94	3	-		< 0.1	-
95	4	-		< 1	-
96	2	-		< 10	-
97	2	$8.4 \cdot 10^2$		80	-
98	2	$1.6 \cdot 10^4$		$1.5 \cdot 10^3$	2
99	2	$2.8 \cdot 10^5$		$2.8 \cdot 10^4$	1
100	2	$1.5 \cdot 10^6$		$1.5 \cdot 10^5$	0.5
101	2	$1.0 \cdot 10^7$	$2.0 \cdot 10^5$	$1.0 \cdot 10^6$	0.5
102	2	$4.5 \cdot 10^7$		$4.5 \cdot 10^6$	0.5
103	2	$2.0 \cdot 10^8$	$1.6 \cdot 10^6$	$2.0 \cdot 10^7$	0.5
104	2	$5.9 \cdot 10^8$		$5.9 \cdot 10^7$	0.5
105	2	$1.3 \cdot 10^9$	$7.0 \cdot 10^7$	$1.3 \cdot 10^8$	0.5
106	2	$1.8 \cdot 10^9$	$7.0 \cdot 10^7$	$1.8 \cdot 10^8$	0.5
107	2	$3.4 \cdot 10^9$		$3.4 \cdot 10^8$	0.5
108	2	$3.5 \cdot 10^9$		$3.5 \cdot 10^8$	0.5
109	2	$5.4 \cdot 10^9$	$6.0 \cdot 10^8$	$5.4 \cdot 10^8$	0.5
110	2	$4.7 \cdot 10^9$		$4.7 \cdot 10^8$	0.5
111	2	$6.4 \cdot 10^9$	$4.0 \cdot 10^9$	$6.4 \cdot 10^8$	0.5
112	1	$4.7 \cdot 10^9$	$2.3 \cdot 10^9$	$4.7 \cdot 10^8$	0.5
113	2	$6.3 \cdot 10^9$	$2.0 \cdot 10^9$	$6.3 \cdot 10^8$	0.5
114	2	$4.6 \cdot 10^9$	$1.0 \cdot 10^9$	$4.6 \cdot 10^8$	0.5
115	2	$5.4 \cdot 10^9$	$1.8 \cdot 10^8$	$5.4 \cdot 10^8$	0.5
116	3	$3.6 \cdot 10^9$		$3.6 \cdot 10^8$	0.5
117	2	$3.8 \cdot 10^9$	$7.0 \cdot 10^8$	$3.7 \cdot 10^8$	0.5
118	3	$1.9 \cdot 10^9$		$1.7 \cdot 10^8$	0.5
119	2	$1.6 \cdot 10^9$		$1.5 \cdot 10^8$	0.5
120	3	$5.6 \cdot 10^8$		$4.3 \cdot 10^7$	0.5
121	2	$3.1 \cdot 10^8$	$3.0 \cdot 10^7$	$2.1 \cdot 10^7$	0.5
122	3	$7.6 \cdot 10^7$		$4.3 \cdot 10^6$	0.5
123	2	$3.5 \cdot 10^7$		$1.2 \cdot 10^6$	0.5
124	2-3?	$8.5 \cdot 10^6$		$1.4 \cdot 10^5$	0.5
125	2	$6.1 \cdot 10^6$		$1.0 \cdot 10^5$	0.5
126	2-3?	$1.5 \cdot 10^6$		$6.4 \cdot 10^2$	4
127	2	$6.5 \cdot 10^5$		$1.4 \cdot 10^3$	3
128	1-3?	$1.1 \cdot 10^5$		62	5
129	2	$1.3 \cdot 10^4$	1	1	7
				Total	35

References

[1] R. Ferrer, N. Bree, T. E. Cocolios, I. G. Darby, H. De Witte, W. Dexters, J. Diriken, J. Elseviers, S. Franchoo, M. Huyse, N. Kesteloot, Y. Kudryavtsev, D. Pauwels, D. Radulov, T. Roger, H. Savajols, P. Van Duppen, and M. Venhart. In-gas-cell laser ionization spectroscopy in the vicinity of ^{100}Sn: Magnetic moments and mean-square charge radii of $N = 50 - 54$Ag. *Phys. Lett. B*, 728:191–197, 2014.

[2] D. Rosiak, M. Seidlitz, P. Reiter, H. Naïdja, Y. Tsunoda, T. Togashi, F. Nowacki, T. Otsuka, G. Colò, K. Arnswald, T. Berry, A. Blazhev, M. J. G. Borge, J. Cederkäll, D. M. Cox, H. De Witte, L. P. Gaffney, C. Henrich, R. Hirsch, M. Huyse, A. Illana, K. Johnston, L. Kaya, Th. Kröll, M. L. Lozano Benito, J. Ojala, J. Pakarinen, M. Queiser, G. Rainovski, J. A. Rodriguez, B. Siebeck, E. Siesling, J. Snäll, P. Van Duppen, A. Vogt, M. von Schmid, N. Warr, F. Wenander, and K. O. Zell. Enhanced quadrupole and octupole strength in doubly magic ^{132}Sn. *Phys. Rev. Lett.*, 121:252501, Dec 2018.

[3] C. Gorges, L. V. Rodríguez, D. L. Balabanski, M. L. Bissell, K. Blaum, B. Cheal, R. F. Garcia Ruiz, G. Georgiev, W. Gins, H. Heylen, A. Kanellakopoulos, S. Kaufmann, M. Kowalska, V. Lagaki, S. Lechner, B. Maaß, S. Malbrunot-Ettenauer, W. Nazarewicz, R. Neugart, G. Neyens, W. Nörtershäuser, P.-G. Reinhard, S. Sailer, R. Sánchez, S. Schmidt, L. Wehner, C. Wraith, L. Xie, Z. Y. Xu, X. F. Yang, and D. T. Yordanov. Laser spectroscopy of neutron-rich tin isotopes: A discontinuity in charge radii across the $n = 82$ shell closure. *Phys. Rev. Lett.*, 122(19):192502, 2019.

[4] V. Manea, J. Karthein, D. Atanasov, M. Bender, K. Blaum, T. E. Cocolios, S. Eliseev, A. Herlert, J. D. Holt, W. J. Huang, Yu. A. Litvinov, D. Lunney, J. Menéndez, M. Mougeot, D. Neidherr, L. Schweikhard, A. Schwenk, J. Simonis, A. Welker, F. Wienholtz, and K. Zuber. First glimpse of the $N = 82$ shell closure below $Z = 50$ from masses of neutron-rich cadmium isotopes and isomers. *Phys. Rev. Lett.*, 124:092502, Mar 2020.

[5] T. D. Morris, J. Simonis, S. R. Stroberg, C. Stumpf, G. Hagen, J. D. Holt, G. R. Jansen, T. Papenbrock, R. Roth, and A. Schwenk. Structure of the lightest tin isotopes. *Phys. Rev. Lett.*, 120:152503, Apr 2018.

[6] B. K. Sahoo, A. R. Vernon, R. F. Ruiz Garcia, C. Binnersley, J. Billowes, M. L. Bissel, T. E. Cocolios, K. T. Flanagan, W. Gins, R. P. de Groote, et al. Analytic response relativistic coupled-cluster theory: The first application to indium isotope shifts. *New Journal of Physics*, 2020.

[7] M. Hammen, W. Nörtershäuser, D. L. Balabanski, M. L. Bissell, K. Blaum, I. Budinčević, B. Cheal, K. T. Flanagan, N. Frömmgen, G. Georgiev, Ch. Geppert, M. Kowalska, K. Kreim, A. Krieger, W. Nazarewicz, R. Neugart, G. Neyens, J. Papuga, P.-G. Reinhard, M. M. Rajabali, S. Schmidt, and D. T. Yordanov. From calcium to cadmium: Testing the pairing functional through charge radii measurements of Cd 100-130. *Phys. Rev. Lett.*, 121(10):102501, 2018.

[8] GK Woodgate and RW Hellwarth. Hyperfine structure of radioactive silver 111Ag. *Proceedings of the Physical Society. Section A*, 69(8):581, 1956.

[9] W. Bruce Ewbank and Howard A. Shugart. Hyperfine-structure measurements on silver-105. *Phys. Rev.*, 129:1617–1621, Feb 1963.

[10] Y.W. Chan, W. Bruce Ewbank, William A. Nierenberg, and Howard A. Shugart. Nuclear spins and hyperfine-structure separations of silver-112 and silver-113. *Phys. Rev.*, 133:B1138–B1144, Mar 1964.

[11] GM Stinson, AR Pierce, JC Waddington, and RG Summers-Gill. Spin and magnetic moment of silver-109m. *Canadian Journal of Physics*, 49(7):906–913, 1971.

[12] W Sahm and A Schwenk. Precision measurements of magnetic moments of nuclei with weak nmr signals. *Zeitschrift für Naturforschung A*, 29(12):1763–1766, 1974.

[13] R. Eder, E. Hagn, and E. Zech. Nuclear magnetic moments of 44.3 s $^{107}\mathrm{Ag}^{\mathrm{m}}$ and 39.8 s $^{109}\mathrm{Ag}^{\mathrm{m}}$. *Phys. Rev. C*, 31:190–196, Jan 1985.

[14] U Dinger, J Eberz, G Huber, R Menges, R Kirchner, O Klepper, T Ku, D Marx, et al. Nuclear moments and change in the charge radii of neutron-deficient silver isotopes. *Nuclear Physics A*, 503(2):331–348, 1989.

[15] A. Vernon. private communications. May 2020.

[16] R. F. Garcia Ruiz, M. L. Bissell, K. Blaum, A. Ekström, N. Frömmgen, G. Hagen, M. Hammen, K. Hebeler, J. D. Holt, G. R. Jansen, M. Kowalska, K. Kreim, W. Nazarewicz, R. Neugart, G. Neyens, W. Nörtershäuser, T. Papenbrock, J. Papuga, A. Schwenk, J. Simonis, K. A. Wendt, and D. T. Yordanov. Unexpectedly large charge radii of neutron-rich calcium isotopes. *Nature Phys.*, 12(6):594, 2016.

[17] P-G Reinhard and W Nazarewicz. Toward a global description of nuclear charge radii: Exploring the fayans energy density functional. *Phys. Rev. C*, 95(6):064328, 2017.

[18] B. A. Marsh, T. Day Goodacre, S. Sels, Y. Tsunoda, B. Andel, A. N. Andreyev, N. A. Althubiti, D. Atanasov, A. E. Barzakh, J. Billowes, K. Blaum, T. E. Cocolios, J. G. Cubiss, J. Dobaczewski, G. J. Farooq-Smith, D. V. Fedorov, V. N. Fedosseev, K. T. Flanagan, L. P. Gaffney, L. Ghys, M. Huyse, S. Kreim, D. Lunney, K. M. Lynch, V. Manea, Y. Martinez Palenzuela, P. L. Molkanov, T. Otsuka, A. Pastore, M. Rosenbusch, R. E. Rossel, S. Rothe, L. Schweikhard, M. D. Seliverstov, P. Spagnoletti, C. Van Beveren, P. Van Duppen, M. Veinhard, E. Verstraelen, A. Welker, K. Wendt, F. Wienholtz, R. N. Wolf, A. Zadvornaya, and K. Zuber. Characterization of the shape-staggering effect in mercury nuclei. *Nature Phys.*, 14(12):1163–1167, 2018.

[19] RP de Groote, Jon Billowes, Corry L Binnersley, Mark L Bissell, Thomas Elias Cocolios, T Day Goodacre, Gregory James Farooq-Smith, DV Fedorov, Kieran T Flanagan, Serge Franchoo, et al. Measurement and microscopic description of odd–even staggering of charge radii of exotic copper isotopes. *Nature Phys.*, pages 1–5, 2020.

[20] Thomas Elias Cocolios. Absolute charge radii of radioactive isotopes measured by muonic x-ray spectroscopy at PSI. (CERN-INTC-2020-024. INTC-P-552), May 2020.

[21] E. Mané, A. Voss, J. A. Behr, J. Billowes, T. Brunner, F. Buchinger, J. E. Crawford, J. Dilling, S. Ettenauer, C. D. P. Levy, O. Shelbaya, and M. R. Pearson. First experimental determination of the charge radius of ^{74}Rb and its application in tests of the unitarity of the cabibbo-kobayashi-maskawa matrix. *Phys. Rev. Lett.*, 107:212502, Nov 2011.

[22] ML Bissell, J Papuga, H Naïdja, K Kreim, Klaus Blaum, M De Rydt, RF Garcia Ruiz, H Heylen, M Kowalska, R Neugart, et al. Proton-neutron pairing correlations in the self-conjugate nucleus k38 probed via a direct measurement of the isomer shift. *Phys. Rev. Lett*, 113(5):052502, 2014.

[23] J. Döring, H. Grawe, K. Schmidt, R. Borcea, S. Galanopoulos, M. Górska, S. Harissopulos, M. Hellström, Z. Janas, R. Kirchner, M. La Commara, C. Mazzocchi, E. Roeckl, and R. Schwengner. Identification of isomers in the Z=N+1 nucleus 95Ag. *Phys. Rev. C - Nuclear Physics*, 68(3):6, sep 2003.

[24] LK Peker, EI Volmyansky, VE Bunakov, and SG Ogloblin. Many-particle isomeric states as sources of proton and neutron radio-activity. *Physics Letters B*, 36(6):547–549, 1971.

[25] R Wadsworth, Nara Singh, Z Liu, H Grawe, T S Brock, P Boutachkov, N Braun, A Blazhev, M Gorska, S Pietri, D Rudolph, C Domingo-Pardo, S J Steer, A Atac, L Bettermann, L Caceres, K Eppinger, T Engert, T Faestermann, F Farinon, F Finke, K Geibel, J Gerl, R Gernhauser, N Goel, A Gottardo, J Grebosz, C Hinke, R Hoischen, G Ilie, H Iwasaki, J Jolie, A Kaskas, I Kojouharov, R Krucken, N Kurz, E Merchan, C Nociforo, J Nyberg, M Pfutzner, A Prochazka, Zs Podolyak, P H Regan, P Reiter, S Rinta-Antila, C Scholl, H Schaffner, P-A Soderstrom, N Warr, H Weick, H-J Wollersheim, P J Woods, F Nowacki, and K Sieja. Spin-gap isomer in 96Cd Related content Spin-gap isomer in 96Cd. *Journal of Physics: Conference Series OPEN ACCESS Journal of Physics: Conference Series*, 381:12074, 2012.

[26] U Köster. Yields and spectroscopy of radioactive isotopes at LOHENGRIN and ISOLDE. Ausbeuten und Spektroskopie radioaktiver Isotope bei LOHENGRIN und ISOLDE, 1999. Presented on 30 Dec 1999.

[27] RF Garcia Ruiz, R Berger, J Billowes, CL Binnersley, ML Bissell, AA Breier, AJ Brinson, K Chrysalidis, T Cocolios, B Cooper, et al. Spectroscopy of short-lived radioactive molecules: A sensitive laboratory for new physics. *arXiv preprint arXiv:1910.13416*, 2019.

[28] RP De Groote, J Billowes, CL Binnersley, ML Bissell, Thomas Elias Cocolios, T Day Goodacre, Gregory James Farooq-Smith, DV Fedorov, KT Flanagan, S Franchoo, et al. Dipole and quadrupole moments of Cu 73–78 as a test of the robustness of the Z=28 shell closure near Ni-78. *Phys. Rev. C*, 96(4):041302, 2017.

Appendix

DESCRIPTION OF THE PROPOSED EXPERIMENT

The experimental setup comprises: (*name the fixed-ISOLDE installations, as well as flexible elements of the experiment*)

Part of the	Availability	Design and manufacturing
CRIS experiment	☒ Existing	☒ To be used without any modification

HAZARDS GENERATED BY THE EXPERIMENT (if using fixed installation:) Hazards named in the document relevant for the fixed CRIS installation.